Photoproductions of $f_1(1285)$ and $\eta'(958)$ from the analysis of CLAS data with the Primakoff effect at high energies

Byung-Geel Yu* and Kook-Jin Kong†

Research Institute of Basic Sciences, Korea Aerospace University, Goyang 10540, Korea

(Received 30 July 2020; accepted 3 September 2020; published 22 September 2020)

We investigate photoproduction of axial vector meson $f_1(1285)$ based on the CLAS experiment $\gamma p \to p f_1(1285) \to p\eta\pi^+\pi^-$ using the Regge model for $\rho^0+\omega$ exchanges. The combined analysis of $\gamma p \to p\eta' \to p\eta\pi^+\pi^-$ reaction including $\eta(1295)$ is accompanied to evaluate the decay mode $\eta(1295) \to \eta\pi^+\pi^-$ from the potential overlap with the f_1 reaction. The predominance of $\rho^0(770)$ exchange over the $\omega(782)$ with the coupling constant $\gamma\rho^0 f_1$ extracted from the CLAS experiment leads to a good description of the measured cross sections for f_1, while the scale of the cross section is corrected by the branching fraction $\eta' \to \eta\pi^+\pi^-$ and $f_1 \to \eta\pi^+\pi^-$, respectively. As an extension to study the nonmesonic production mechanism, the Primakoff effect by the virtual photon exchange is investigated in the exclusive reaction $\gamma p \to p f_1$ up to $\sqrt{s} \approx 50$ GeV, playing role similar to the Pomeron in the vector meson photoproduction at high energies. Such a unique role of the virtual photon exchange similar to the f_1 case is identified up to $\sqrt{s} \approx 250$ GeV in the $\gamma p \to p\pi^0$ and $\gamma p \to p\eta$ as well as $\gamma p \to p\eta'$ reactions.

DOI: 10.1103/PhysRevD.102.054019

I. INTRODUCTION

The axial vector meson $f_1(1285)$ of spin-isospin and parity quantum numbers $I^G J^{PC} = 0^+(1^{++})$ has many interesting aspects from the standpoint of QCD; a saturating trajectory of f_1 Regge pole associated with QCD axial anomaly [1] and its application to elastic pp scattering and vector meson photoproductions [2,3] are the most interesting topics of QCD at high energies together with the central production of f_1 meson via the double photon fusion $\gamma^*\gamma^* \to f_1$ in the leptonic [4] and hadronic diffraction processes [5]. Besides those issues through the reactions, the Primakoff effect $f_1 \to \gamma^*\gamma$ [6] and the branching ratio $f_1 \to a^0\pi \approx 36\%$, which is large enough to study the exotic four-quark state $a_0(980)$ [7], are closely related to the study of quark structure of mesons. Moreover, the decay width $\Gamma_{f_1} = 22.7 \pm 1.1$ MeV from the Particle Data Group (PDG) (and 18.4 ± 1.4 MeV from the recent measurement by the CLAS Collaboration [8]) is much smaller than the typical meson decay width, which can be advantageous in finding the formation of exotics such as $\pi_1(1400)$ via the $\gamma p \to \Delta\pi_1 \to p\eta\pi\pi$ process [9–14].

Recent reports of differential cross sections for $\gamma p \to p f_1(1285)$ measured from the reaction $\gamma p \to p\eta\pi^+\pi^-$ by the CLAS Collaboration [8] drew our attention because it is the first measurement to provide information on the static and dynamical properties of f_1 meson that can access the above issues through theoretical studies and comparisons of experiments on f_1 photoproduction. On the other hand, however, the existing models that predict f_1 photoproduction [15,16] using the $\rho^0+\omega$ Regge poles in the t channel disagree with CLAS experimental data. This is mainly because their contributions with the anomaly coupling constants of $\gamma\rho^0 f_1$ (and $\gamma\omega f_1 \approx \frac{1}{3}\gamma\rho^0 f_1$) determined from the PDG are too large to be consistent with data. Furthermore, since the exclusive reaction $\gamma p \to p f_1$ should be reconstructed through the multimeson production in the final state from the aforementioned CLAS data, experimental circumstances such as the branching ratio $f_1 \to \eta\pi^+\pi^-$ should be considered in the analysis of CLAS data for the single process $\gamma p \to p f_1$.

In this work, we investigate photoproduction of f_1 based on the CLAS data of the reaction $\gamma p \to p\eta\pi^+\pi^-$ using a Reggeized model for $\rho^0+\omega$ exchanges. We recall that the data were extracted from the experiment in which case the interference of $\eta(1295)$ photoproduction was neglected in the region overlapping with $f_1(1285)$. Viewed from the PDG, productions of η' and $\eta(1295)$ as well as $f_1(1285)$ are other sources of decay to $\eta\pi^+\pi^-$, so the reactions $\gamma p \to p\eta'$ and $\gamma p \to p\eta(1295)$ are also involved in the reaction $\gamma p \to p\eta\pi^+\pi^-$. Thus, we examine the respective contributions of η' and $\eta(1295)$ photoproductions to the

*bgyu@kau.ac.kr
†kong@kau.ac.kr

CLAS data first, starting from photoproductions of these η's. The f_1 photoproduction will then be described with the trajectories of $\rho^0+\omega$ Regge poles and their VNN coupling constants the same as in the case of η and η'. The reliability of model prediction is confirmed by the roles of $\rho^0+\omega$ Regge poles in the η and η' cases, which were rather well established in previous studies [17,18]. In the model study of f_1 photoproduction, the ρ^0 exchange plays the leading role over the ω. Therefore, it is of importance to consider the decay width $f_1\to\rho^0\gamma$ more appropriate for a consistent description of CLAS data. As mentioned earlier, the PDG value is very large, and there is a significant difference from the one extracted from the CLAS experiment. In Ref. [6], this issue was revisited to evaluate the decay width $f_1\to\rho^0\gamma$ based on the well-known triangle diagram for the AVV coupling vertex. The quark loop calculation using Bose symmetry and gauge invariance yields the decay width $f_1\to\rho^0\gamma$ much smaller than the PDG value, supporting the one extracted from the CLAS experiment [8].

In addition to the vector meson exchange, we consider another subprocess of nonmesonic exchange that has different energy dependence from vector mesons. By the C-even property of the f_1 meson and η as well, the virtual photon of C odd is allowed to exchange in the t channel the so-called the Primakoff effect that manifests itself at very forward angles as a rapid enhancement in the differential cross section [19,20]. In the energy range of the CLAS experiment where the vector meson exchanges are dominant, the Primakoff effect is expected to be suppressed by the charge coupling with the nucleon. Nevertheless, since the exchange of the virtual photon is not to be Reggeized, its role could become significant at high energy, where there is decrease of vector meson exchange according to the energy dependence of approximately $s^{\alpha_V(0)-1}$.

Now that the Primakoff effect in the photoproduction of η and of η' is related to the flavor mixing of η-η' (the theme of the PrimEx project at CLAS [21] and the current upgrade to GlueX at CLAS12), measurements of the Primakoff effect in the reaction can give clues to understanding the structure of the flavor symmetry, e.g., the mixing of flavor octet and singlet between η-η', and so is the mixing between $f_1(1285)$ and $f_1(1420)$ [22]. This point will be addressed in the context of the two-gamma decay in the photoproduction of pseudoscalar meson π^0, η, and η' and will be extended to the Primakoff effect in the $\gamma p\to pf_1$ reaction at high energies.

This paper is organized as follows. In Sec. II, photoproductions of η, η', and $\eta(1295)$ on the proton target are investigated in the Reggeized model for $\rho^0+\omega$ exchanges. Section III is devoted to an analysis of the exclusive f_1 photoproduction on proton from the multimeson reaction $\gamma p\to p\eta\pi^+\pi^-$ within the same approach as in Sec. II. Differential and total cross sections for the CLAS experiment are reproduced in Sec. III.A. Predictions for the energy dependence of differential cross section and the beam polarization asymmetry are presented to distinguish between the reactions aforementioned for future experiments. The Primakoff effect by the virtual photon exchange is studied in the photoproduction of f_1 in Sec. III.B., and π^0, η, and η' cases are studied in Sec. III. C. A summary and conclusion are given in Sec. IV.

II. PHOTOPRODUCTIONS OF $\eta(548)$, $\eta'(958)$, AND $\eta(1295)$ ON THE PROTON TARGET

As the threshold energies of the exclusive processes $\gamma p\to p\eta(1295)$ and $\gamma p\to pf_1(1285)$ are over the region $\sqrt{s}_{\rm thres}\approx 2.2$ GeV, the contribution of nucleon resonances in the direct and crossed channels are not expected, and, hence, it is good to consider only the t-channel meson exchange for the description of these reactions.

In this section, we treat the photoproduction of η' and $\eta(1295)$ in a single framework where the vector meson exchange is Reggeized with vector meson nucleon coupling constants (VNN) common in all the reactions we are dealing with in the current work. For consistency, let us start from $\gamma p\to p\eta(548)$ to provide a basic formalism which will be extended to η' and $\eta(1295)$ with each radiative decay constant determined from the empirical decay width for the different η mass.

For the exclusive η photoproduction on nucleon,

$$\gamma(k)+N(p)\to\eta(q)+N(p'), \tag{1}$$

we denote the particle momenta k, q, p, and p' to stand for the incident photon, outgoing η meson, and initial and final nucleons, respectively. $s=(p+k)^2$ and $t=(q-k)^2$ are the Mandelstam variables in the reaction kinematics. We restrict our discussion only to the production mechanism by the meson exchange, as depicted in Fig. 1, for our purpose here is to see how the meson exchange works well in the kinematical region of $\eta(1295)$ and $f_1(1285)$ photoproductions.

The photoproduction amplitude for the exchange of C-odd vector meson on nucleon is written as

$$M(\gamma N\to N\eta)=\pm\rho+\omega, \tag{2}$$

with the sign of ρ for proton and neutron, respectively.

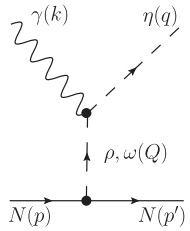

FIG. 1. ρ and ω exchanges in the exclusive η photoproduction. $Q^\mu=(q-k)^\mu$ denotes the momentum transfer and $Q^2=t$ in the t channel.

The effective Lagrangians for the vector meson exchange is written as

$$\mathcal{L}_{VNN} = \bar{N}\left(g^v_{VNN}\gamma^\mu + \frac{g^t_{VNN}}{2M}\sigma^{\mu\nu}\partial_\nu\right)V_\mu N \tag{3}$$

$$\mathcal{L}_{\gamma\eta V} = \frac{g_{\gamma\eta V}}{4m_0}\epsilon_{\mu\nu\alpha\beta}F^{\mu\nu}V^{\alpha\beta}\eta + \text{H.c.}, \tag{4}$$

and the corresponding production amplitude is given by

$$\mathcal{M}_V = \frac{g_{\gamma\eta V}}{m_0}\epsilon_{\mu\nu\alpha\beta}\epsilon^\mu k^\nu Q^\alpha\left(-g^{\beta\rho} + \frac{Q^\beta Q^\rho}{m_V^2}\right)\bar{u}'(p') \times\left(g^v_{VNN}\gamma_\rho + \frac{g^t_{VNN}}{4M}[\gamma_\rho, \not{Q}]\right)u(p)\mathcal{R}^V(s,t). \tag{5}$$

Here, ϵ^μ is the incident photon polarization, and $Q^\mu = (q-k)^\mu$ is the momentum transfer in the t channel with $Q^2 = t$. The coupling constant is normalized by the mass parameter m_0 chosen to be 1 GeV.

The Regge pole for spin-1 vector meson is given by

$$\mathcal{R}^V(s,t) = \frac{\pi\alpha'_V \times \text{phase}}{\Gamma[\alpha_V(t)]\sin\pi\alpha_V(t)}\left(\frac{s}{s_0}\right)^{\alpha_V(t)-1} \tag{6}$$

for the vector meson $V(=\rho,\omega)$ collectively.

The choice of ρ trajectory is not unanimous. Viewed from the reactions [23,24] where the single ρ exchange is involved to test its role, it is better to choose ρ trajectory as

$$\alpha_\rho(t) = 0.9t + 0.46, \tag{7}$$

$$\alpha_\omega(t) = 0.9t + 0.44 \tag{8}$$

and for the ω trajectory as well with the coupling constants $g^v_{\rho NN} = 2.6$ and $g^t_{\rho NN} = 9.62$. For the ωNN couplings, we use $g^v_{\omega NN} = 15.6$ and $g^t_{\omega NN} = 0$ consistent with the ratio $f_\rho : f_\omega = 1:3$ by the vector meson dominance.

The radiative decay constant $g_{\gamma\eta V}$ is determined from the measured decay width,

$$\Gamma_{V\to\eta\gamma} = \frac{1}{96\pi}\frac{g^2_{\gamma\eta V}}{m_0^2}\left(\frac{m_V^2 - m_\eta^2}{m_V}\right)^3. \tag{9}$$

For the process $\gamma p \to p\eta'$ and $\gamma p \to p\eta(1295)$ in which cases the decay modes are reversed, i.e., $\eta'(\eta(1295)) \to V$, the decay width in Eq. (9) is multiplied by the factor of 3 to recover the initial $\eta'(\eta(1295))$ spin degree of freedom.

Given the trajectories in Eqs. (7) and (8) together with the ratios $g_{\gamma\eta\rho}/g_{\gamma\eta\omega} \simeq 4$ and $2g^v_{\rho NN}/g^v_{\omega NN} \simeq 1/3$ in Table I, the ω exchange is expected to give the contribution quite the same as the ρ, if the same phase is taken. This observation could be valid for η' and $\eta(1295)$ as well within the present framework. We choose the complex phase $e^{-i\pi\alpha_V(t)}$ for both ρ and ω Reggeons in the case of proton target because there is no dip from the nonsense zeros of the Regge poles in the differential cross section data [25–27]. This agrees with the general features of reaction cross sections. For the reaction $\gamma n \to n\eta$, we take the constant phase 1 for ρ and -1 for ω Reggeons for a better description of the total cross section.

TABLE I. Compilation of coupling constants used for the eta-maid [17] and Regge model [15] for η photoproduction. Radiative coupling constant $g_{\gamma\eta V}$ is given in units of GeV^{-1}.

	η-MAID [17]	Regge model [15]	This work
$g_{\gamma\eta\rho}$	0.448	⋯	0.448
$g_{\gamma\eta'\rho}$	0.392	⋯	0.36
$g_{\gamma\eta(1295)\rho}$	⋯	0.0566	0.0566
$g^v_{\rho NN}$	2.4	3.9	2.6
$g^t_{\rho NN}$	8.88	23.79	9.62
$g_{\gamma\eta\omega}$	0.16	⋯	0.106
$g_{\gamma\eta'\omega}$	−0.136	⋯	0.12
$g_{\gamma\eta(1295)\omega}$	⋯	0.0189	0.0189
$g^v_{\omega NN}$	9	10.6	15.6
$g^t_{\omega NN}$	0	0	0

To illustrate the validity of the $\rho+\omega$ Reggeon exchanges for the reaction $\gamma N \to N\eta$, we present the scaled differential cross section by the factor $(s-M^2)^2$ reproduced at $E_\gamma =$ 3 GeV (solid curve), beam polarizations at $E_\gamma = 3$ GeV (dot-dashed) and $E_\gamma = 9$ GeV (solid), and the respective total cross sections for $\gamma p \to p\eta$ and $\gamma n \to n\eta$ as well in Fig. 2. The (red) dashed and (blue) dot-dashed curves correspond to the ρ and ω Reggeon contributions to differential and total cross sections from a proton target, respectively. As mentioned before, they play the role roughly equal to each other. A few remarks are in order: η photoproduction is sensitive to a choice of phase of Reggeon as well as the ρ trajectory between $\alpha_\rho = 0.8t + 0.55$ and that in Eq. (7). In the former case, it is advantageous to choose one of the Reggeons, i.e., ω, to have the exchange-nondegenerate phase. But in that case, the contribution of the ω is suppressed, and the production mechanism resulting from the dominance of ρ over the ω would be quite different from the present one as shown in Fig. 2.

Meanwhile, most of the Regge models for η photoproduction introduce hadron form factors at the $\gamma\eta V$ and VNN vertices to fit to experimental data [17]. However, it is natural to dispense with such form factors in the Regge amplitude because it contains the gamma function $\Gamma(\alpha_V(t))$ in Eq. (6) to suppress the singularity from the sequential zeros of $\sin\pi\alpha_V(t)$. Thus, as demonstrated in Figs. 5 and 6, the present approach without form factors is less model dependent than those in Refs. [15,16] to describe the CLAS data.

Next, we calculate the exclusive $\gamma p \to p\eta'$ and $\eta(1295)$ within the same framework. However, in order to compare

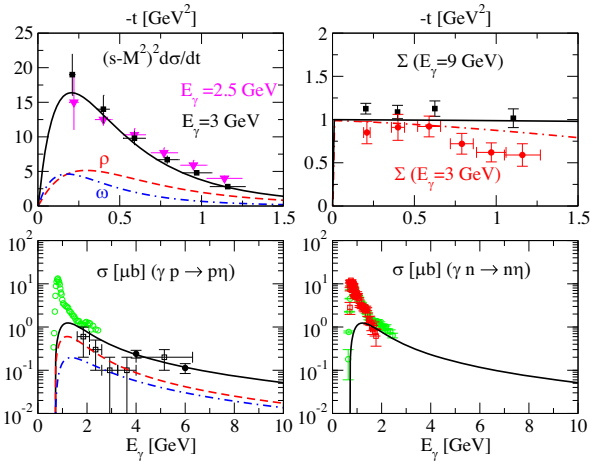

FIG. 2. Scaled differential cross section, beam polarization, total cross sections for $\gamma p \to p\eta$, and total cross section for $\gamma n \to n\eta$. The solid curve results from $\rho^0 + \omega$ Reggeon exchanges. Scaled differential cross section at $E_\gamma = 3$ GeV is shown with data taken from Ref. [28] and for beam polarization with respect to $-t$ at $E_\gamma = 3$ GeV [28] and at 9 GeV [11]. Data for $p\eta$ total cross section at $E_\gamma = 4$ and 6 GeV are from the integration of DESY differential data in Ref. [25], and open squares in the $1.6 \le E_\gamma \le 6.3$ GeV are from AHHM Collaboration data in Ref. [29]. Data for resonance peaks are from the world dataset [30–32].

with the CLAS data from the multimeson photoproduction process $\gamma p \to \eta(958)p \to p\eta\pi^+\pi^-$, we consider the branching ratio $\Gamma_{\eta'\to\eta\pi^+\pi^-}/\Gamma_{\eta'\to all} \approx 43\%$, from the PDG to implement the reduction by an overall factor of 0.43 to the cross section from the exclusive process $\gamma p \to p\eta'$. In Table I, we list the coupling constants compiled for the η' and $\eta(1295)$ in addition to η photoproduction above. For the physical status of $\eta(1295)$, only the mass $m_{\eta(1295)} = 1294 \pm 4$ MeV and decay width $\Gamma_{\eta(1295)} = 55 \pm 5$ MeV are known. We follow the coupling constants deduced from Ref. [15] to calculate total cross section with the same ratio of the reduction as in the case of η'.

Figures 3 and 4 show the differential and total cross section for η' and total cross section for $\eta(1295)$. As before, the complex phase $e^{-i\pi\alpha}$ is chosen for both $\rho + \omega$ Reggeons in both reactions. Data of differential cross sections are from the CLAS measurement, and the data for the total cross section in Fig. 4 are from the AHHM [29]. These reaction cross sections are scaled, as discussed above. The angular distribution reproduced in Fig. 3 is consistent with data. Nevertheless, in addition to the t-channel exchanges, the underestimate of differential data below $\sqrt{s} \approx 2.55$ GeV implies the need for the contribution of baryon resonances in the s and u channels in order to reproduce the backward rise as well as the forward enhancement in the cross section. As for the total cross sections in Fig. 4, we first note that the model prediction without correction is consistent with the exclusive AHHM cross section [29] as shown by the dashed curve. Within the present framework, the $\eta(1295)$ cross section is smaller

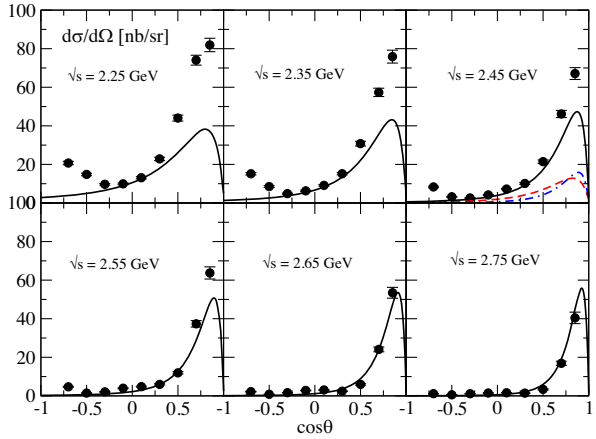

FIG. 3. Differential cross section $d\sigma/d\Omega$ vs $\cos\theta$ for $\gamma p \to p\eta'(958)$. The solid curve results from $\rho + \omega$ Reggeon exchanges with a factor of 0.43 taken into account for the branching fraction from the $\gamma p \to p\eta\pi^+\pi^-$ experiment. Below $\sqrt{s} \approx 2.55$ GeV, there is a room for nucleon resonances to contribute to the backward rise as well as the forward enhancement. Notations for ρ and ω contributions are the same as in Fig. 2. Data are taken from Ref. [8].

than the η' by 2 orders of magnitude, and, hence, it is reasonable to neglect the $\eta(1295)$ production in the data analysis for f_1 production from the reaction $\gamma p \to p\eta\pi^+\pi^-$, as performed by the CLAS Collaboration.

III. $f_1(1285)$ PHOTOPRODUCTION ON THE PROTON TARGET

A. Analysis of CLAS data from $\gamma p \to p f_1 \to p\eta\pi^+\pi^-$ below $\sqrt{s} = 3$ GeV

In the CEBAF Large Acceptance Spectrometer (CLAS) experiment on the $\gamma p \to p\eta\pi^+\pi^-$ reaction, the structure of

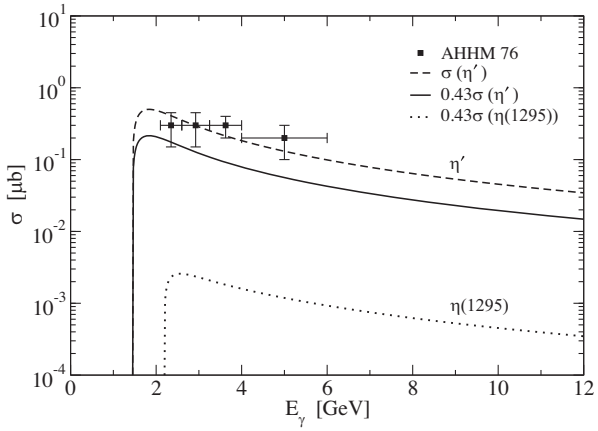

FIG. 4. Total cross sections for $\gamma p \to p\eta'$ and $\gamma p \to p\eta(1295)$. The solid and dotted curves correspond to η' and $\eta(1295)$ production cross sections scaled by the branching ratio. For comparison, the dashed curve for the η' cross section without scaling is presented to reproduce the AHHM data [29].

$f_1(1285)$ was observed at $m_X \simeq 1280$ MeV of the γp missing mass spectrum with a great statistics $\simeq 1.5 \times 10^5 \times (1280)$ events. Since $\eta(1295)$ as well as $f_1(1285)$ are decaying to $\eta\pi\pi$, care must be taken for the potential overlap with each other to extract the structure associated with the $f_1(1285)$ with p-wave decay and positive parity from the Dalitz analysis of $x \to \eta\pi^+\pi^-$. The experiment leads to a conclusion on f_1 with mass $m_{f_1} = 1281.0 \pm 0.8$ MeV and width $\Gamma_{f_1} = 18.4 \pm 1.4$ MeV, which is narrower than the PDG value 24.2 ± 1.1 MeV.

On the theoretical side, Kochelev *et al.* [15] and Domokos *et al.* [16] calculated the reaction cross section for the exclusive $\gamma p \to p f_1$ reaction, using the Reggeized model for the t-channel ρ and ω vector meson exchanges with the hadron form factor of the form, either $\left(\frac{\Lambda^2 - m_V^2}{\Lambda^2 - t}\right)^n$ assigned to the $\gamma V f_1$ and VNN vertices [15] or the overall form factor $(1 - t/0.71)^{-2}$ [16].

As depicted in Fig. 1 in which the outgoing η meson is now replaced by the f_1 meson in the Feynman diagram, we consider the $\rho + \omega$ meson exchanges similar to those models above but exclude such form factors for consistency with the reactions involved in ηs. The form of the γVA coupling vertex

$$\Gamma^{\beta}_{\gamma VA}(k, Q)\eta_\beta = \frac{g_{\gamma VA}}{m_0^2} Q^2 \epsilon^{\mu\nu\alpha\beta} \epsilon_\mu k_\nu \xi^*_\alpha \eta_\beta, \tag{10}$$

is utilized from Ref. [15] for the t-channel vector meson exchange. Here, $\xi^\alpha(q)$ and $\eta^\beta(Q)$ are spin polarizations of axial vector meson and vector meson with the momenta q and Q, respectively. Given the VNN coupling vertex in Eq. (3), the vector meson exchange is now written as

$$\mathcal{M}_V = \Gamma^{\beta}_{\gamma VA}(k, Q)(-g_{\beta\lambda} + Q_\beta Q_\lambda / m_V^2)\bar{u}(p') \times \left(g^v_{VNN}\gamma^\lambda + \frac{g^t_{VNN}}{4M}[\gamma^\lambda, \not{Q}]\right) u(p)\mathcal{R}^V(s,t) \tag{11}$$

with the decay width of the γVA vertex corresponding to Eq. (10) given by

$$\Gamma_{A\to V\gamma} = \frac{1}{96\pi}\frac{g^2_{\gamma VA}}{m_0^4}\frac{m_V^2}{m_A^5}(m_A^2 + m_V^2)(m_A^2 - m_V^2)^3. \tag{12}$$

For the coupling vertex $\gamma\rho^0 f_1$, Ref. [15] determined $g_{\gamma\rho^0 f_1} = 0.94$ from the decay width $\Gamma_{f_1\to\rho^0\gamma} \approx 1330$ keV presently reported by the PDG. The coupling constant $g_{\gamma\omega f_1} = -g_{\gamma\rho f_1}/3$ is taken from the quark model estimation. However, with the trajectories and VNN coupling constants given in Ref. [15], the model prediction for the CLAS data is poor, even though the model assumes the reduction of the calculated cross section by the branching ration 35% as applied in Figs. 3 and 4 for comparison with the CLAS cross section $\gamma p \to p f_1 \to p\eta\pi^+\pi^-$. The crucial point of the issue is that the PDG width $f_1 \to \rho^0\gamma$ chosen above is too large to agree with the CLAS data. Theoretical estimates based on the QCD inspired models such as the constituent quark model (CQM) [33] and the four-quark state with the triangle loop for the AVV anomaly [6] suggest half the value of the current PDG fit. Moreover, the width 453 ± 177 keV extracted from the CLAS experiment further supports these smaller values rather than the PDG one as shown in Table II.

TABLE II. Estimate of γVA coupling constant from the decay width of Ref. [8][a], Ref. [33][b], Ref. [6], and PDG, which are given in units of keV. For comparison, we list $g_{\gamma\rho f_1} = 0.59^b$, 0.45^c, and 0.94^d. $g_{\gamma\omega f_1} = 0.152^c$ from these references.

	$g_{\gamma VA}$	CLAS [8]	CQM [33]	4-quark [6]	PDG
$f_1 \to \rho\gamma$	0.54^a	453^a	509^b	311^c	1330^d
$f_1 \to \omega\gamma$	-0.18^b	⋯	48^b	34.3^c	⋯

We perform the analysis of the CLAS data with the decay width $\Gamma_{f_1\to\rho^0\gamma} = 453$ keV determined from the CLAS experiment. We then demonstrate how the production mechanism could account for the CLAS data, while comparing our results with Ref. [15]. It is legitimate to consider simply the $\rho^0 + \omega$ exchanges as in Fig. 1 because threshold energy of the reaction, $\sqrt{s}_{\rm thres} \approx 2.2$ GeV, is high enough to neglect nucleon resonances. This might be a contradiction to the finding in Ref. [8] that the production mechanism is more consistent with s-channel decay of a high-mass N^* state not with t-channel meson exchange because the hadron models aforementioned are insufficient to reproduce the CLAS data. The role of nucleon resonance $N^*(2300)(1/2^+)$ together with the nucleon in the s and u channels is discussed to account for the u-channel rise at $\sqrt{s} = 2.65$ and 2.75. [34]. Nevertheless, it should be pointed out that the results from these models follow the dependence on the cutoff mass of the form factors, which is the point that is quite different from the current calculation.

In Table II, we choose $g_{\gamma\rho f_1} = 0.54$ from the CLAS width and $g_{\gamma\omega f_1} = -0.18$ from the relativistic quark model, which resumes the ratio of $g_{\gamma\rho^0 f_1}/g_{\gamma\omega f_1} \approx -3$.

With the VNN coupling constants in Table I and the vector meson trajectories in Eqs. (7) and (8), we reproduce the CLAS differential cross section in Fig. 5. To describe the exclusive $\gamma p \to p f_1$ reaction from the CLAS data which are extracted from the $\gamma p \to p\eta\pi^+\pi^-$ in the final state, we have to consider a scaling of the cross section by the fraction $\Gamma_{f_1\to\eta\pi^+\pi^-}/\Gamma_{f_1\to all} \approx 0.35$, similar to the case of η' photoproduction, as before. As the differential cross section data show no oscillatory behavior, the complex phase $e^{-i\pi\alpha_\rho(t)}$ for the ρ is mandatory, and the canonical phase $1/2(-1 + e^{-i\pi\alpha_\omega(t)})$ is chosen for ω to be consistent with data. The roles of ρ and ω are displayed at $\sqrt{s} = 2.55$ GeV. The (green) dot-dashed curve results

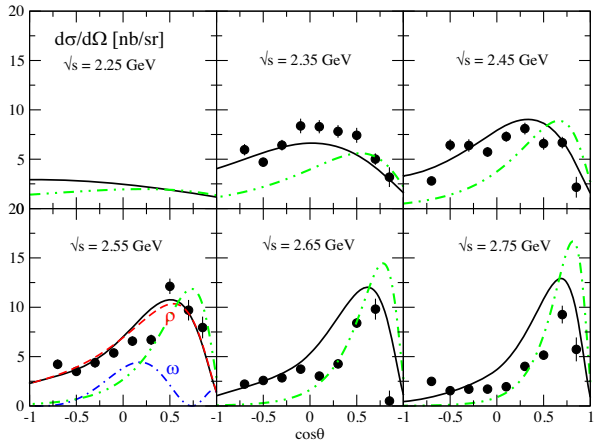

FIG. 5. Differential cross section $d\sigma/d\Omega$ vs $\cos\theta$ for $\gamma p \to p f_1 \to p\eta\pi^+\pi^-$. The solid cross sections are scaled by a factor of 0.35 to account for the branching fraction from the $\gamma p \to p\eta\pi^+\pi^-$. The (green) dot-dot-dashed curve is from Ref. [15] with $\Lambda_1 = 1.2$ and $\Lambda_2 = 1.4$ GeV and $n = 1$ for the $\gamma V f_1$ form factor. Data are taken from Ref. [8].

from Ref. [15] with the cutoff masses $\Lambda_1 = 1.2$ and $\Lambda_2 = 1.4$ GeV together with $n = 1$ for the form factors. In the model, only $g_{\gamma V f_1}$ is taken the same as ours for comparison. It is shown that the cross section is too suppressed in the nonforward direction due to the form factors, which is different from the present approach without form factors.

Total cross sections for f_1 and $\eta(1295)$ photoproductions are shown in Fig. 6. For reference purposes, the five total cross section data are obtained through the integration of differential cross section data in Fig. 5 and compared with the model calculation. The difference between our model

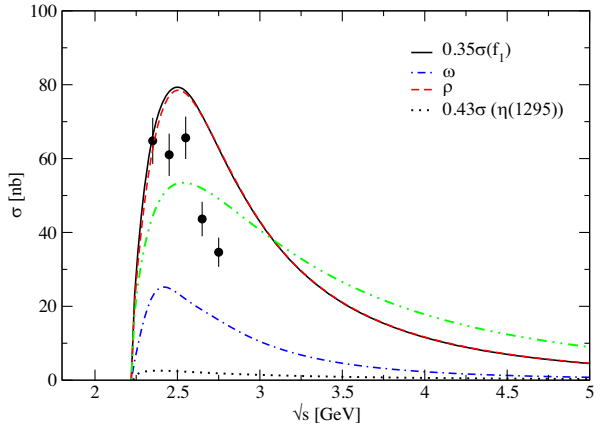

FIG. 6. Total cross sections for $\gamma p \to P f_1 \to p\eta\pi^+\pi^-$ and $\gamma p \to p\eta(1295) \to p\eta\pi^+\pi^-$. Five data points in the f_1 cross section are obtained by integrating out the differential cross sections given in Fig. 5 for illustration purposes. The cross sections are scaled by the same factors as in Figs. 4 and 5, respectively. For comparison the cross section for f_1 from Ref. [15] is presented by the green dash-dot-dotted curve. The cross section for $\gamma p \to \eta(1295)p$ scaled by 43% is shown to be negligible in the region overlapping with f_1 production.

prediction and cross section is understood to be probably due to differential cross section data not being sufficient. However, it is interesting to see in Ref. [34] that the total cross section is given similarly to our case in shape and magnitude, insofar as the model prediction agrees with differential cross section data in its own way. The respective contributions of ρ and ω exchanges are shown with the same notations. The dot-dot-dashed curve from Ref. [15], as in Fig. 5, yields the smaller cross section at low energy. The cross section for $\eta(1295)$ photoproduction is shown with a correction by the factor of 0.43. By comparison, we agree with the negligence of the $\eta(1295)$ component in the CLAS analysis of $f_1(1285)$ cross section from the reaction $\gamma p \to p\eta\pi^+\pi^-$.

For further studies on the CLAS data, we present the energy dependence of differential cross section at the forward angle $\theta = 40°$ (corresponding to a forward peak at $\cos\theta \approx 0.75$ and $\sqrt{s} = 2.75$ GeV in Fig. 5) in Fig. 7 for $f_1(1285)$, $\eta(958)$, and $\eta(1295)$ cross sections involved in the overlapped potential region. The discrimination between these reactions is more apparent in the beam polarization Σ as can be seen in Fig. 7. As the present model includes only the natural parity exchange of ρ and ω, the Σ is always positive. But the different size of the Σ between pseudoscalar and axial vector meson photoproductions reveals the different scheme of the interference between ρ and ω Reggeons among these reactions.

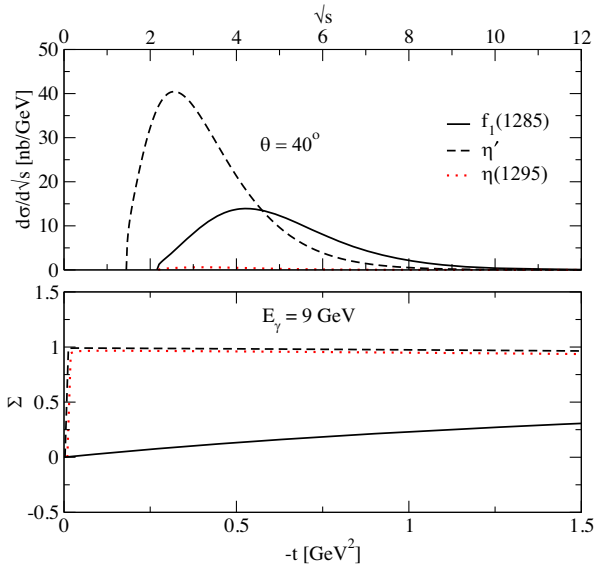

FIG. 7. Differential cross section and beam polarization asymmetry for f_1, η', and $\eta(1295)$ photoproductions from the CLAS experiment $\gamma p \to p\eta\pi^+\pi^-$. Differential cross sections scaled by the respective factors are predicted as a function of $\sqrt{s}$ at the production angle $\theta^* = 40°$ in the center of mass system. The t-dependence of beam polarizations are presented at $E_\gamma = 9$ GeV with the same notation as in the differential cross sections.

B. Primakoff effect in the f_1 process

Now that the decay $f_1 \to \gamma^*\gamma$ is another source of the reaction $\gamma p \to p f_1$ to proceed in the forward direction, the virtual photon exchange contributes to the exclusive f_1 photo-production via one of the two photons off mass shell in the t channel. This is the so-called the Primakoff effect, which is observed at very forward angles, in general, in the photoproduction of charge-neutral meson of C-parity even [19,20]. The Primakoff effect provides an opportunity to test nonperturbative properties of QCD through the mixing of the nonet members in the axial anomaly [21]. Moreover, as the virtual photon exchange is not to be Reggeized, it is not subject to the energy dependence $s^{\alpha(0)-1}$ at high energies. Therefore, by virtue of it, such energy-independent behavior is expected in the reaction, as in the case of the Pomeron exchange at high energies in vector meson photoproduction. The nature of the Pomeron and virtual photon exchange is, of course, quite different. The origin of the former process comes from strong interaction by the exchange of two gluon correlation [35], whereas the latter exchange results from the axial anomaly in the presence of electromagnetic interaction. Thus, this subprocess in the t channel will be an example of seeking the nonmesonic process that can survive at high energies in the photoproduction of axial vector meson.

Before proceeding, some comment is needed to clarify the anomaly couplings between $f_1(1285) \to \gamma^*\gamma^*$ and $f_1(1285) \to \gamma^*\gamma$, which are important for the Primakoff effect in various reactions. According to Ref. [4], the anomaly coupling of the former process found in the literature is not definite so far, and, hence, a correct form of the coupling vertex should be pinned down by precise experiments. However, such a discussion is relatively limited here because the latter vertex $f_1 \to \gamma^*\gamma$ in our case has an external real photon coupling. Rosenberg [36] and Close [37] suggested the coupling form, which is applicable to the present work and proved to be equivalent to the order p^3 terms in the quark loop calculation of the anomaly triangle diagram [6].

Given the γVA vertex in Eq. (10), we replace the vector meson polarization η_β by the virtual photon ϵ'_β with 4-momentum Q^μ in the t channel for the virtual photon exchange. Then, the γ^* exchange is written as

$$\mathcal{M}_{\gamma^*} = -\Gamma^{\beta}_{\gamma\gamma^* A}(k,Q)F_\rho(t)\frac{(-g_{\beta\lambda})}{t}e\bar{u}(p') \times \left(e_N\gamma^\lambda + \frac{\kappa_N}{4M}[\gamma^\lambda, \not{Q}]\right)F_1(t)u(p), \quad (13)$$

where the coupling constant $g_{\gamma VA}$ in Eq. (10) is read as $g_{\gamma\gamma^* A}$ and the vector meson polarization η_β is read as ϵ'_β with the vector meson propagator and VNN vertex replaced by the virtual photon propagator and γ^*NN vertex in Eq. (11). e_N equals 1 for a proton with $\kappa_p = 1.79$ and 0 for a neutron with $\kappa_n = -1.91$. The coupling constant $g_{\gamma\gamma^* A}$ now in Eqs. (10) and (13) cannot be estimated from the decay width as before because of vanishing of Q^2 for the case of a real photon. This is also the result of the Landau-Yang theorem [38]. In practice, the evaluation of the $f_1 \to \gamma^*\gamma$ vertex is rather complicated [39]. Following Ref. [6], the form factor $F^{(0)}_{AV\gamma^*\gamma^*}(m_f^2, Q^2, k^2)$ for the vertex $f_1 \to \gamma^*\gamma^*$ was measured in the case of real photons, $f_1 \to \gamma\gamma$. To utilize this, it is reasonable to consider the form factor $F^{(0)}_{AV\gamma^*\gamma^*}(m_f^2, Q^2, 0)$ in our case as being given by the form $F^{(0)}_{AV\gamma^*\gamma^*}(m_f^2, 0, 0)F_\rho(Q^2)$, with its Q^2 dependence provided by the vector meson dominance, i.e., by the ρ-meson pole

$$F_\rho(t) = (1 - t/m_\rho^2)^{-1}. \quad (14)$$

Thus, the coupling constant can be written as

$$\frac{g_{\gamma\gamma^* A}}{m_0^2} = 8\pi\alpha F^{(0)}_{AV\gamma^*\gamma^*}(m_f^2, 0, 0) \quad (15)$$

in Eq. (13), and we obtain $g_{\gamma\gamma^* f_1} = 0.043$ by taking $F^{(0)}_{AV\gamma^*\gamma^*}(m_f^2, 0, 0) = (0.234 \pm 0.034)\,\mathrm{GeV}^{-2}$ from the PDG.

Since we are dealing with the virtual photon exchange coupling to the isoscalar f_1 meson, the nucleon isoscalar form factor

$$F_1(t) = \frac{4M^2 - 2.8t}{(4M^2 - t)(1 - t/0.71\ \mathrm{GeV}^2)^2} \quad (16)$$

is introduced to γ^*NN vertex in the t channel.

By the vector meson dominance, a combination of $\rho - \omega - \phi$ meson poles should be applied to the $\gamma\gamma^* f_1$ vertex with the mixing between $\rho + \omega$ and ϕ vector mesons as discussed in Ref. [19] for the cases of $\gamma\gamma^*\eta$ and $\gamma\gamma^*\eta'$ vertices. Suppose that there is no difference between vector meson masses; then, these form factors lead roughly to a unity as the mixing has no meaning between $\rho + \omega$ and ϕ [19]. Thus, we choose the ρ-meson pole here as a representative for simplicity. For the γ^*NN vertex, we employ the nucleon isoscalar form factor in Eq. (16), which replaces the Dirac form factors F_1 and F_2, as discussed in Ref. [40]. The form factors in Eqs. (14) and (16) with cutoff masses are well established in other hadronic processes so that we have no model dependence in calculating reaction cross sections for the $\gamma p \to p f_1$ reaction.

In Fig. 8, the differential cross section is presented at forward angles below $\theta = 35°$ at $\sqrt{s} = 6$ GeV, and the total cross section is shown up to $\sqrt{s} \approx 50$ GeV in Fig. 9. Since there is no information about the sign of the $\gamma\gamma^* f_1$ coupling relative to that of the vector meson exchange, $\gamma V f_1$, the cross section is shown for both signs of $g_{\gamma\gamma^* f_1}$ for illustration purposes. The solid and dashed (red) curves are from the full calculation of the differential and total

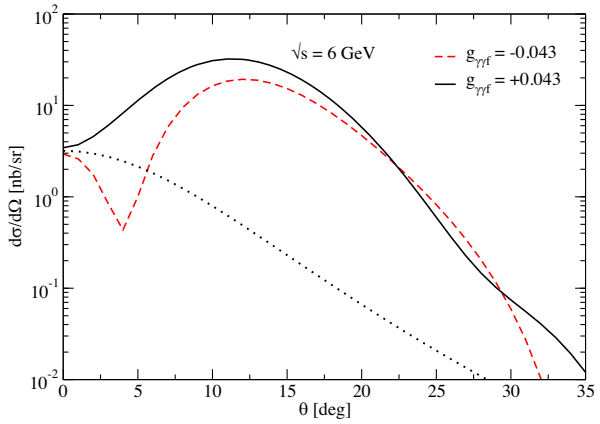

FIG. 8. Differential cross section for the exclusive $\gamma p \to p f_1$ reaction as a function of angle θ. The dotted curve represents the contribution of γ^* exchange. The Primakoff effect between the positive and negative signs of the coupling constant $f_{\gamma\gamma^* f_1}$ shows a different angle dependence below $\theta \approx 5°$.

cross sections corresponding to positive and negative signs. The exchange of γ^* is denoted by the dotted curve in both cross sections.

It is found that in the total cross section the role of form factor $F_\rho(t)$ in Eq. (14) is negligible. However, without the nucleon isoscalar form factor $F_1(t)$, the cross section is highly divergent, as can be seen by the dot-dashed curve. The energy dependence of the cross section shows a growth of the Primakoff effect up to $\sqrt{s} \approx 5$ GeV and remains constant, i.e., $\sigma \approx 0.1$ nb up to $\sqrt{s} \approx 50$ GeV. Beyond $\sqrt{s} \approx 25$ GeV, the contribution of γ^* exchange becomes stronger than those of vector meson exchanges which are decreasing by the energy dependence of approximately $s^{\alpha_V(0)-1}$.

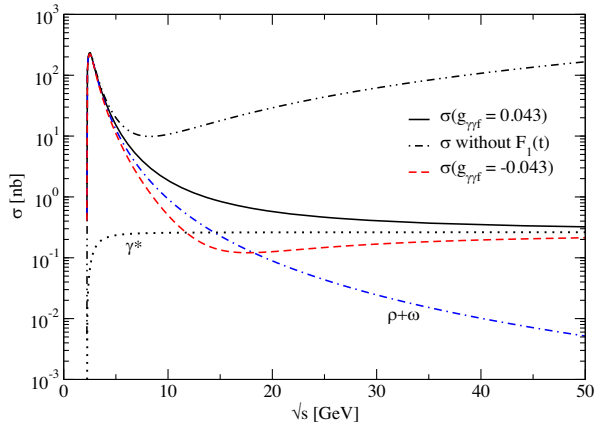

FIG. 9. Total cross section for the exclusive $\gamma p \to p f_1$ process up to $\sqrt{s} = 50$ GeV. Contributions of γ^* and $\rho + \omega$ exchanges are shown by the dotted and dot-dashed curves, respectively. The solid (dashed) curve corresponds to total cross section with the relative sign of γ^* exchange positive (negative) to vector meson exchanges. The exchange of γ^* gives the contribution $\sigma \approx 0.25$ nb at $\sqrt{s} \approx 50$ GeV persistent up to the higher energies. The solid cross section without form factor $F_1(t)$ diverges, as shown by the dot-dot-dashed curve.

C. Primakoff effect in pseudoscalar meson photoproduction

Pseudoscalar meson photoproduction is a typical reaction to observe the Primakoff effect by the γ^* exchange [19,20]. A precise measurement of the Primakoff effect has been advocated to test the nonperturbative QCD based on the flavor mixing of the chiral symmetry [21]. Here, we shall reproduce the Primakoff effect in the photoproduction of π^0 and η as well as η' in the PrimEx energy region [21] and compare the result with the data available. Nevertheless, our interest in this issue is still more in understanding the role of the nonmesonic scattering in the pseudoscalar meson photoproduction at high energies, as demonstrated in the f_1 photoproduction.

For the Primakoff effect, the virtual photon exchange in the η photoproduction is written as

$$\mathcal{M}_{\gamma^*} = \frac{f_{\gamma\gamma^*\eta}}{m_\eta} F_{\gamma\gamma^*\eta}(t) \epsilon^{\mu\nu\alpha\beta} \epsilon_\mu k_\nu Q_\alpha \frac{(-g_{\beta\lambda})}{t} e\bar{u}(p') \times \left(e_N \gamma^\lambda + \frac{\kappa_N}{4M} [\gamma^\lambda, \not{Q}] \right) F_1(t) u(p), \tag{17}$$

where the vertex form factors $F_{\gamma\gamma^*\eta}(t)$ and $F_1(t)$ are given by Eqs. (14) and (16), respectively. The radiative coupling constant $f_{\gamma\gamma^*\eta}$ is estimated from the decay width

$$\Gamma_{\eta\to\gamma\gamma} = \frac{f^2_{\gamma\gamma\eta} m_\eta}{64\pi} \tag{18}$$

with the PDG value taken for the $\eta \to \gamma\gamma$ decay.

In Fig. 10, the differential cross sections for $\gamma p \to p\eta$ with the DESY data [25] and $\gamma p \to p\eta'$ and $\gamma p \to p\pi^0$ [41] are presented to exhibit the role of γ^* exchange at very forward angles. The solid curve results from the $\rho + \omega + \gamma^*$ exchanges in Eqs. (5) and (17) with $f_{\gamma\gamma^*\eta}/m_\eta = -0.014/m_\eta$ from $\Gamma_{\eta\to\gamma\gamma} = 0.52$ keV, $f_{\gamma\gamma^*\eta'}/m_{\eta'} = -0.03/m_{\eta'}$ from $\Gamma_{\eta'\to\gamma\gamma} = 4.28$ keV, and $f_{\gamma\gamma^*\pi^0}/m_{\pi^0} = +0.00342/m_{\pi^0}$ from $\Gamma_{\pi^0\to\gamma\gamma} = 7.74$ eV cases [42]. The coupling constants $g_{\gamma\pi^0\rho} = 0.255$ and $g_{\gamma\pi^0\omega} = 0.7$ are used for the π^0 cross sections with the VNN coupling constants given in Table I. The trajectories are taken the same as the η case, but the phases $e^{-i\pi\alpha_\rho}$ and $\frac{1}{2}(-1 + e^{-i\pi\alpha_\omega})$ are chosen for ρ^0 and ω, respectively. In the case of η, the negative sign is chosen for the constructive interference between γ^* and $\rho + \omega$ exchanges. However, the result shows a discrepancy with experimental data, in particular, below $\theta \approx 5°$, which is comparable to that of Ref. [19] at the same energy. To agree with the data, the coupling constant $f_{\gamma\gamma^*\eta}$ should grow by three times larger than the one given above, as shown by the

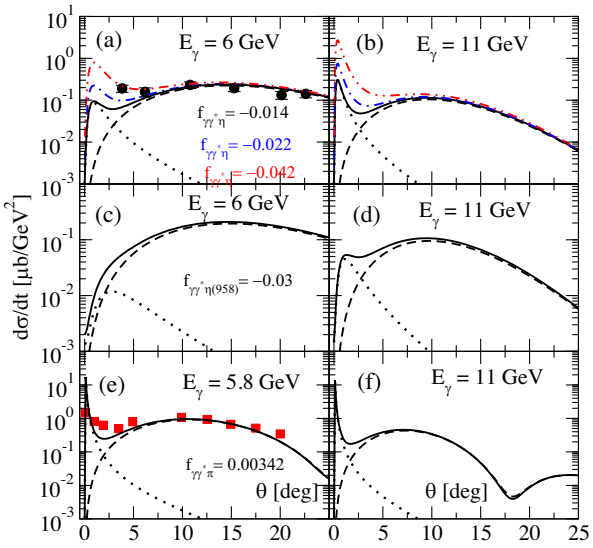

FIG. 10. Differential cross sections for $\gamma p \to p\eta$ in (a) and (b), $\gamma p \to p\eta'$ in (c) and (d), and $\gamma p \to p\pi^0$ in (e) and (f). The (red) dot-dot-dashed, (blue) dot-dashed, and solid curves result from the case of coupling constant $f_{\gamma\gamma^*\eta}$ as denoted in panel (a), respectively. In (f), the dip at $\theta \approx 18°$ is due to the nonsense zero of ω exchange. Data of η and of π^0 production are taken from Refs. [25,41], respectively.

(red) dot-dot-dashed curve. In this case, the result is similar to Ref. [20]. This is, however, unattainable, even though the maximum value for the mixing angle is chosen between η_0 and η_8, when we express the decay width $\eta \to \gamma\gamma$ and $\eta' \to \gamma\gamma$ as in Eqs. (19) and (20) given below.

In consideration of the mixing of the $SU_f(3)$ flavor singlet and octet members, the decay widths for $\eta \to \gamma\gamma$ and $\eta' \to \gamma\gamma$ are written as [21]

$$\Gamma_{\eta\to\gamma\gamma} = \frac{\alpha^2}{64\pi^3}\frac{m_\eta^3}{3f_\pi^2}\left(\frac{f_\pi}{f_{\eta_8}}\cos\theta_p - \sqrt{8}\frac{f_\pi}{f_{\eta_0}}\sin\theta_p\right)^2, \tag{19}$$

$$\Gamma_{\eta'\to\gamma\gamma} = \frac{\alpha^2}{64\pi^3}\frac{m_{\eta'}^3}{3f_\pi^2}\left(\frac{f_\pi}{f_{\eta_8}}\sin\theta_p + \sqrt{8}\frac{f_\pi}{f_{\eta_0}}\cos\theta_p\right)^2, \tag{20}$$

where f_{η_0} and f_{η_8} are the flavor singlet and octet decay constants and θ_p is the mixing angle for pseudoscalar mesons. They are estimated as $f_{\eta_8} \approx 1.3 f_\pi$ by Chiral perturbation theory(ChPT) and $f_{\eta_0} \approx f_\pi$ in the large N_c limit. The ratio measured in the experiment

$$R = \frac{1}{3}\left(\frac{f_\pi^2}{f_{\eta_8}^2} + 8\frac{f_\pi^2}{f_{\eta_0}^2}\right) = 2.5 \pm 0.5 \tag{21}$$

is consistent with the theoretical estimates, $f_\pi/f_{\eta_0} = 0.93$ with $f_\pi/f_{\eta_8} = 1/1.3$.

Let us now make an estimate of the decay width based on Eqs. (19) and (20). In terms of $f_{\eta_0} = 100.1$ MeV and $f_{\eta_8} = 121$ MeV that are given by taking $f_\pi = 93.1$ MeV above, the η decay width 0.52 keV taken here corresponds to the mixing angle $\theta_p \approx -23.4°$. At the angle, the corresponding η' decay width leads to 4.03 keV from Eq. (20), which is close to the empirical value quoted above. In practice, the maximum angle θ_p in Eq. (19) exists at $-74°$ (or 106°), which yields the decay width 1.27 keV. The (blue) dot-dashed curve corresponds to the decay width at such an angle θ_p with $f_{\gamma\gamma^*\eta} = -0.022$, which is, however, still deficient to agree with data. Moreover, in that case, the η' decay width from Eq. (20) is vanishing, i.e., about 0.2 eV at the angle. Therefore, from the relations between η and η' mixing above, the coupling constant $f_{\gamma\gamma^*\eta} = |0.042|$ cannot be achievable, and we notice that the discrepancy below the production angle $\theta \approx 5°$ can no longer be covered over even with the mixing angle maximally allowed. In future experiments such as the PrimEX project at CLAS 12 GeV, a precise measurement of the cross section at very forward angles is desirable to decide whether such a disagreement is still due to a theoretical deficiency or an experimental uncertainty.

Figure 11 shows total cross sections for $\gamma p \to p\pi^0$, $\gamma p \to p\eta$, and $\gamma p \to p\eta'$ reactions up to $\sqrt{s} \approx 250$ GeV. The solid cross sections are from the $\rho + \omega + \gamma^*$ exchanges in the t channel. Beyond $\sqrt{s} \approx 100$ GeV where there exists the dominating γ^* exchange, the π^0 and η cross sections are persistently scaled to a common limit $\sigma \simeq 1.5$ nb around $\sqrt{s} \simeq 250$ GeV. This coincidence is understood, if one notes that $f_{\gamma\gamma^*\pi^0} \approx f_{\gamma\gamma^*\eta}$ in the unit of GeV^{-1}. The η' cross section reaches the limit $\sigma \simeq 2.2$ nb with the coupling constant larger than those of π^0 and η'. Together with the f_1 case as shown in Fig. 9, the role of γ^* exchange in these cross sections scaling up to 250 GeV can be

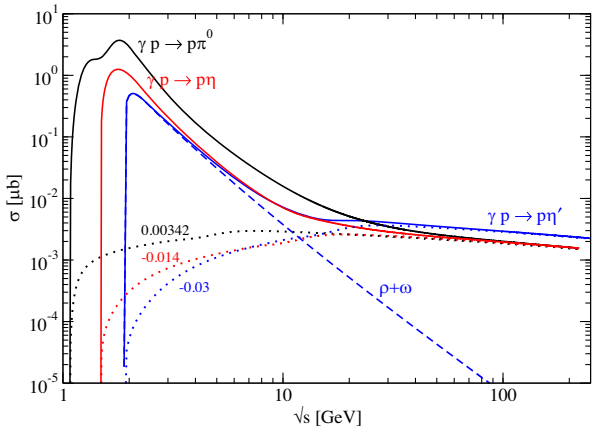

FIG. 11. Primakoff effect in $\gamma p \to p\pi^0$, $\gamma p \to p\eta$ and $\gamma p \to p\eta'$ reactions at high energies. The dotted curve is the contribution of γ^* exchange which shows a nearly energy independent behavior up to $\sqrt{s} \approx 250$ GeV. The rapid peak of the total cross section near threshold is reproduced by the $\rho + \omega$ exchanges depicted by the dashed curve in the η' process, for instance.

compared to that of the Pomeron exchange in the vector meson photoproduction. The limit of the cross section at high energies is determined only by the coupling strength of each meson decaying to two gammas. Therefore, a measurement of the η and η' cross sections at such limiting energies enables us to determine the mixing angles from Eqs. (19) and (20).

Before closing this section, we would like to give a remark on the specialty of photoproductions of the pseudoscalar and axial vector meson, which exhibits the dynamical features as interesting as the Pomeron exchange in the vector meson photoproduction at high energies. Of course, in these reactions, besides the virtual photon exchange, we note that there is an important mechanism to prove QCD, called the exchange of Odderon, which can be another entity comparable to the Pomeron [43,44]. Like the Pomeron exchange in the high-energy vector meson photoproduction, the search of the Odderon is a most interesting topic for studying the role of odd numbers of gluons in hadron reactions. Thus, predicting the γ^* exchange as in Figs. 9 and 11 should be important to find out the Odderon exchange in future experiments, if available at such high energies. This topic will be our next work, which will appear elsewhere.

IV. SUMMARY

The first half of the present work is devoted to analyzing CLAS data on the η' and $f_1(1285)$ photoproductions based on the $\rho + \omega$ Reggeon exchanges. The observables of η photoproduction are reproduced to confirm the validity of the vector meson contributions, prior to the studies of the η' and $\eta(1295)$ photoproductions. To describe the exclusive reaction $\gamma p \to p\eta'$ from the multimeson photoproduction in the final state $\gamma p \to p\eta\pi^+\pi^-$, and similarly in the case of $\eta(1295)$, the reaction cross section is corrected by the branching ratio, taking into account the final decay mode reported in the PDG. The Regge calculation of axial vector meson $f_1(1285)$ photoproduction is performed within the same framework. It is found that the $\eta(1295)$ photoproduction is small enough to be neglected in the reconstruction of $\gamma p \to p f_1$ from the reaction $\gamma p \to p\eta\pi^+\pi^-$. Our model could reproduce the differential cross section to a good degree, if the branching ratio for $f_1 \to \eta\pi^+\pi^-$ of 35% and the decay width 453 keV are feasible to use. To demonstrate the production mechanism different between pseudoscalar and axial vector meson photoproduction, predictions for the energy dependence of differential cross sections and the t dependence of the beam polarization asymmetry are presented. In particular, the beam polarization asymmetry shows the features quite contrasting each other.

The rest of the present work is focused on the exclusive f_1 photoproduction with a special interest in the search of nonmesonic scattering process such as the Pomeron exchange in the vector meson photoproduction. The Primakoff effect by the virtual photon exchange shows the behavior of energy independence at high energies so that the total cross section remains constant persistently up to $\sqrt{s} \approx 50$ GeV with the size of $\sigma \approx 2$ nb. This feature from the virtual photon exchange is also implemented in the pseudoscalar meson photoproduction with the cross section approaching to the limiting value 1.5 nb in the π^0 and η and 2.2 nb in the η' cases at high energies.

These results provide useful information for the study of the Primakoff effect by the PrimEX project at CLAS 12 GeV, and also the detailed analysis of $\gamma p \to p\eta\pi^+\pi^-$ reaction presented in this work helps search for exotic mesons via multimeson photoproduction in the GlueX project at Jefferson Laboratory.

ACKNOWLEDGMENTS

This work was supported by the National Research Foundation of Korea Grant No. NRF-2017R1A2B4010117.

[1] N. I. Kochelev, D.-P. Min, Y. Oh, V. Vento, and A. V. Vinnikov, Phys. Rev. D **61**, 094008 (2000).
[2] B.-G. Yu, T. K. Choi, and K.-J. Kong, J. Phys. G **46**, 075005 (2019).
[3] B.-G. Yu, H. Kim, and K.-J. Kong, Phys. Rev. D **95**, 014020 (2017).
[4] A. Szczurek, arXiv:2006.01516.
[5] P. Lebiedowicz, J. Leutgeb, O. Nachtmann, A. Rebhan, and A. Szczurek, arXiv:2008.07452.
[6] A. A. Osipov, A. A. Pivovarov, and M. K. Volkov, Phys. Rev. D **96**, 054012 (2017).
[7] V. R. Debastiani, F. Aceti, W.-H. Liang, and E. Oset, Phys. Rev. D **95**, 034015 (2017).
[8] R. Dickson *et al.* (CLAS Collaboration), Phys. Rev. C **93**, 065202 (2016).
[9] A. P. Szczepaniak, Eur. Phys. J. A **18**, 167 (2003).
[10] C. A. Meyer and E. S. Swanson, Prog. Part. Nucl. Phys. **82**, 21 (2015).
[11] H. Al Ghoul *et al.* (GlueX Collaboration), Phys. Rev. C **95**, 042201(R) (2017).
[12] A. P. Szczepaniak and M. Swat, Phys. Lett. B **516**, 72 (2001).
[13] J. Kuhn *et al.*, Phys. Lett. B **595**, 109 (2004).
[14] D. Schott, AIP Conf. Proc. **1257**, 492 (2010).
[15] N. I. Kochelev, M. Battaglieri, and R. De Vita, Phys. Rev. C **80**, 025201 (2009).

[16] S. K. Domokos, H. R. Grigoryan, and J. A. Harvey, Phys. Rev. D **80**, 115018 (2009).
[17] W.-T. Chiang, S. N. Yang, L. Tiator, M. Vanderhaeghen, and D. Drechsel, Nucl. Phys. **A700**, 429 (2002); Phys. Rev. C **68**, 045202 (2003).
[18] L. Tiator, M. Gorchtein, V. L. Kashevarov, K. Nikonov, M. Ostrick, M. Hadžimehmedović, R. Omerović, H. Osmanović, J. Stahov, and A. Švarc, Eur. Phys. J. A **54**, 210 (2018).
[19] M. M. Kaskulov and U. Mosel, Phys. Rev. C **84**, 065206 (2011).
[20] A. Sibirtsev, J. Haidenbauer, S. Krewald, and U.-G. Meißner, Eur. Phys. J. A **44**, 169 (2010).
[21] A. Gasparian, L. Gan, J. Goity, D. Dale, M. Ito, D. Lawrence, A. Margarian, R. Miskimen, A. Bernstein, S. Danagoulian, D. Klabucar (PrimEx Collaboration), Draft, *Precision Measurements of the Electromagnetic Properties of Pseudoscalar Mesons at 11 GeV via the Primakoff Effect* (2000).
[22] K.-C. Yang, Phys. Rev. D **84**, 034035-1 (2011).
[23] B.-G. Yu and K.-J. Kong, Phys. Lett. B **765**, 221 (2017).
[24] K.-J. Kong and B.-G. Yu, Phys. Rev. C **98**, 045207 (2018).
[25] W. Braunschweig, W. Erlewein, H. Frese, K. Lübelsmeyer, H. Meyer-Wachsmuth, D. Schmitz, A. Schultz von Dratzig, and G. Wessels, Phys. Lett. B **33**, 236 (1970).
[26] J. Dewire, B. Gittelman, R. Loe, E. C. Loh, D. J. Ritchie, and R. A. Lewis, Phys. Lett. B **37**, 326 (1971).
[27] V. Crede *et al.* (CBELSA/TAPS Collaboration), Phys. Rev. C **80**, 055202 (2009).
[28] P. J. Bussey *et al.*, Phys. Lett. B **61**, 479 (1976).
[29] W. Struczinski *et al.* (AHHM Collaboration), Nucl. Phys. **B108**, 45 (1976).
[30] I. Jaegle *et al.* (CBELSA/TAPS Collaboration), Phys. Rev. Lett. **100**, 252002 (2008).
[31] V. Crede *et al.* (CBELSA/TAPS Collaboration), Phys. Rev. Lett. **94**, 012004 (2005).
[32] V. Crede *et al.* (CBELSA/TAPS Collaboration), Phys. Rev. C **80**, 055202 (2009).
[33] S. Ishida, K. Yamada, and M. Oda, Phys. Rev. D **40**, 1497 (1989).
[34] Y.-Y. Wang, L.-J. Liu, E. Wang, and D.-M. Li, Phys. Rev. D **95**, 096015 (2017).
[35] P. V. Landshoff and O. Nachtmann, Z. Phys. C **35**, 405 (1987).
[36] L. Rosenberg, Phys. Rev. **129**, 2786 (1963).
[37] F. E. Close, Phys. Lett. B **419**, 387 (1998).
[38] L. D. Landau, Dokl. Akad. Nauk SSSR **60**, 207 (1948); C. N. Yang, Phys. Rev. **77**, 242 (1950).
[39] R. N. Cahn, Phys. Rev. D **35**, 3342 (1987).
[40] A. Donnachie and P. V. Landshoff, Nucl. Phys. **B231**, 189 (1984).
[41] M. Braunschweig, W. Braunschweig, D. Husmann, K. Lübelsmeyer, and D. Schmitz, Nucl. Phys. **B20**, 191 (1970).
[42] C. Amsler *et al.* (Particle Data Group), Phys. Lett. B **667**, 1 (2008).
[43] E. R. Berger and O. Nachtmann, Nucl. Phys. B, Proc. Suppl. **79**, 352 (1999); E. R. Berger, arXiv:hep-ph/9905519.
[44] C. Adloff *et al.*, Phys. Lett. B **544**, 35 (2002).